IEEE Access
Multidisciplinary | Rapid Review | Open Access Journal

Received March 17, 2019, accepted April 20, 2019, date of publication April 26, 2019, date of current version May 7, 2019.

Digital Object Identifier 10.1109/ACCESS.2019.2913592

Force-Sensing Robotic Microinjection System for Automated Multi-Cell Injection With Consistent Quality

ZHIJIE NAN[1], QINGSONG XU[1], (Senior Member, IEEE), YIBO ZHANG[2], AND WEI GE[2]
[1]Department of Electromechanical Engineering, Faculty of Science and Technology, University of Macau, Macau, China
[2]Centre of Reproduction, Development and Aging, Faculty of Health Sciences, University of Macau, Macau, China

Corresponding authors: Qingsong Xu (qsxu@um.edu.mo) and Wei Ge (weige@um.edu.mo)

This work was supported in part by the National Natural Science Foundation of China under Grant 51575545, in part by the Macao Science and Technology Development Fund under Grant 179/2017/A3, and in part by the Research Committee of University of Macau under Grant MYRG2018-00034-FST.

ABSTRACT This paper presents the design and development of a new microinjection system with force sensing for automated multi-cell injection in genome editing of zebrafish using the CRISPR/Cas9 system. In comparison with the traditional approach, it achieves a high injection speed and high precision of operation, which leads to consistent quality and high survival rate of the injected cells. One unique feature is that force sensing is employed to determine the exact moment when the cell membrane is pierced, which contributes to the protection of the cell from damage. Moreover, a new cell holding device is designed to immobilize the cells, which speeds up the multi-cell microinjection process by eliminating the use of conventional vacuum holding pipette. The system implements the object detection by machine vision algorithm along with position/force regulation. The machine vision is realized by combining the pyramid template matching algorithm with Kalman filter, which reduces the computation time and facilitates real-time control. The experimental studies are conducted to verify the performance of the developed system. Results demonstrate the reliability of the robotic microinjection system, which offers a more consistent injection quality and higher viability of cells over the skilled human operator.

INDEX TERMS Microinjection, machine vision, force sensing, microrobotics, automation, biomedical engineering.

I. INTRODUCTION

Cell microinjection is the process of injecting extraneous material into a biological cell. It plays a crucial role in gene editing, intracytoplasmic sperm injection (ICSI), drug delivery, etc. The cells in biology can be classified into two types including adherent and suspended cells. This paper is focused on the injection of suspended cells. In majority of biomedical engineering laboratories, the microinjection operation of suspended cells is currently conducted by skilled human operators, because it is the simplest method to achieve micro-scale operations, such as cell selection and drug injection [1], [2]. The advantage of manual operation lies in that the operator can detect the emergency situations and know how to solve the problems (e.g., removing dead cells, selecting a position that is more close to the fertilized egg for drug injection, etc.). However, the shortage of manual operation mainly includes nonrepeatability, low precision, and high cost on operator training [3], [4]. To overcome such issues, robotic technologies have been employed to automate the operation, such as drug injection [5], [6], cell translation and rotation [7], pick-and-place operation [8], [9], and so on. The reason lies in that robotic devices exhibit several advantages in micro/nano-scale operation in terms of high precision, no-rest operation, low training time, and liberation of human labors [10].

The conventional robotic microinjection system realizes the cell injection by using stand-alone motion control without considering the injecting force [11], [12]. Recently, it has been demonstrated that the force regulation is important to reduce the injury of the injected cell [13]. Microforce sensing is beneficial for the cell microinjection process by providing the real-time force signal [14]. Traditionally, the microforce

The associate editor coordinating the review of this manuscript and approving it for publication was Gursel Alici.

sensing is implemented by vision-based approach [15], [16]. By monitoring the deformation from the acquired images, the force can be calculated via a cell model. Although vision-based position sensing is fine for motion control purpose, vision-based force sensing exhibits several disadvantages. For instance, a vision-based force sensor is heavily dependent on the availability of suitable cell model, and a priori knowledge of the cell mechanical properties should be generated before estimating the force [17], [18]. However, establishing and identifying reliable mechanical models for different kinds of cells are impossible, as the mechanical behavior of soft cells is complicated (e.g., viscoelastic, elastic, nonlinear, and time-varying). Different types of microforce sensors have been developed by researchers, as reviewed in the previous work [19]. Nevertheless, no suitable commercial force sensor is available at the market for microinjection operation [20], [21].

In the literature, several custom-built force sensors have been reported for the use in cell microinjection. For instance, Lu *et al.* [20] have employed a micropipette which is glued vertically on the end of a cantilever-type piezoresistive micro-force sensor for cell penetration. However, foreign material cannot be delivered into the cells by such device. In addition, a force sensor using simply supported polyvinylidene fluoride (PVDF) beam structure has been introduced by Xie *et al.* [22], [23], where the cell injection approach based on force control is developed to regulate the penetration force. However, the aforementioned work is aimed at single cell microinjection and the cell immobilization is not considered explicitly. To implement multi-cell injection, a suitable cell holding device is demanded to immobilize the cells for a reliable cell injection. The conventional method employs a vacuum pipette holder, which is able to hold one cell at a time [24], [25]. To speed up the injection process, several multi-cell holders have been presented to immobile a batch of cells at the same time. For example, Huang *et al.* [26] have proposed a circular-shape cell holding device with concentric grooves. Lu *et al.* [27] have designed a cell holder using a well array with through-holes. However, negative and positive pressures are required to immobile and release the cells via sealed chamber, which demands an extra precision vacuum pump.

To this end, an automated microinjection system is developed with custom-built microforce sensor for automated injection of multiple cells in this work. Specifically, the force sensor is designed based on piezoresistive strain-gauge, which is more stable than PVDF in static force measurement in microinjection. A new cell holding device is proposed to immobile multiple cells simply in V-groove array. In comparison with existing designs, the presented cell holder provides a low-cost and effective approach for immobilizing cells without using an extra vacuum pump. An entire microinjection system is developed which is capable of auto-searching and detecting target cells, injecting drug into cells, judging whether the cell is injected or not, and protecting the cell with force monitoring. The designed piezoresistive strain-gauge force sensor is employed to measure the injecting force during the cell membrane piercing process. The force signal is adopted to guarantee that the cell will not be damaged during the injection process. A machine vision algorithm which combines pyramid template matching and Kalman filter is proposed to detect the target cell, which increases the object matching speed while keeping the accuracy. By integrating the cell holding device with the automatic cell searching method, the developed system is capable of injecting more than 200 zebrafish embryos in one setup. Experimental studies have been performed to demonstrate the superior performance of the developed system in comparison with skilled human operator (with over three years' experience) for microinjection task.

The major contribution of the paper is the development and application of a new force-sensing microinjection system for automated injection of multiple cells dedicated to genome editing of zebrafish. Unlike the authors' previous work [13], a comprehensive microinjection system has been developed in the current work. Moreover, a new cell holding device is proposed to immobile multiple cells simply in V-groove array, and a combined machine vision algorithm is introduced to reduce the processing time. The following parts of the paper are organized as follows. Section II presents the system development process. The machine vision approach for object detection is implemented in Section III. Section IV outlines the experimental studies and results. Section V concludes the paper.

II. SYSTEM DEVELOPMENT AND EXPERIMENTAL SETUP

A computer-aided design (CAD) model of the designed flexure-based compliant injector is shown in Fig. 1(a). It is driven by a stack-type piezoelectric actuator (PZT) [13]. In addition to the role of motion guiding, the injector

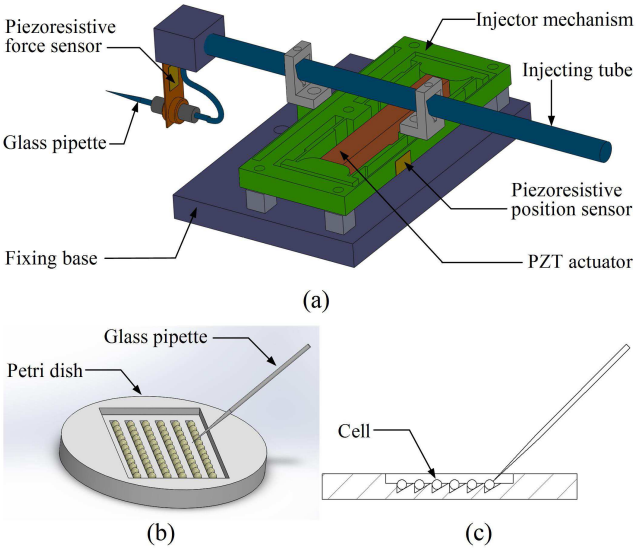

FIGURE 1. CAD model of the designed cell injector (a) and cell holder with 3D view (b) and side view (c).

mechanism also functions as a displacement amplifier in order to amplify the output stroke of the PZT. The glass pipette is supported by a cantilever type of microforce sensor, which is designed to measure the injecting force of biological cell. The PZT is introduced to provide a rapid piercing motion for the cell without excessive deformation, which is benefit to the improvement of cell's survival rate.

For a reliable cell injection, the cells to be injected need to be fixed firmly. The mostly employed method is the vacuum pipette, which is able to hold one cell at a time. Considering the convenience and versatility, a new cell holder with grooves is fabricated (see Fig. 1(b)) to immobilize the cells in this work. As shown in Fig. 1(c), several grooves with triangular cross-section are fabricated on the cell holder. The depth of the grooves is designed according to the diameter of injected cells, such that the cells will not move when the injection pipette pierces into them. To make full use of the space, the cells are placed closely line by line in the petri dish. The fabricated prototype and experimental setup are shown in Fig. 2(a). In comparison with existing multi-cell holder designs [26], [27], no extra negative and positive pressures are required to immobile and release the cells, which provides a more cost-effective approach.

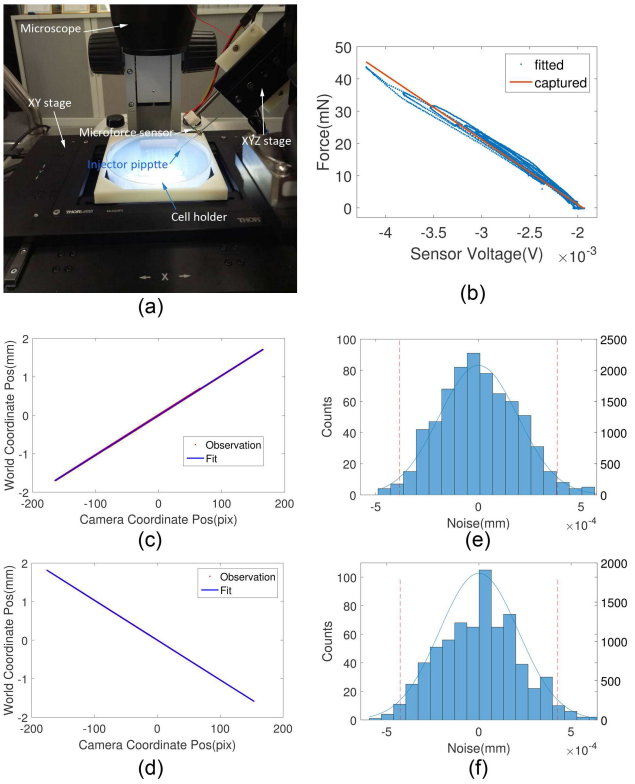

FIGURE 2. (a) Prototype of the developed microinjection system; (b) calibration result of the force sensor; vision-based calibration results in (c) *x*-axis and (d) *y*-axis; noise distribution of the position obtained by the object detection algorithm in (e) *x*-axis and (f) *y*-axis.

The fabrication of the system components is presented in the following.

A. FABRICATION OF THE SYSTEM COMPONENTS

1) FABRICATION OF MICROPIPETTE

The micropipette is fabricated by heating and pulling borosilicate glass capillary tubes (model: 1B100-4, from World Precision Instruments, Inc.) with a micropipette puller device (model: Flaming/Brown P-1000, Sutter Instruments, Inc.).

2) FABRICATION OF FORCE-SENSING INJECTOR

The flexure-based compliant injector mechanism is fabricated with Al 7075 alloy via the wire-electrical discharge machining approach. The Al alloy material is chosen owing to its relatively high elasticity and light mass density. The force sensor is constructed by gluing a piezoresistive strain gauge on the surface of a PVDF film. The piezoresistive sensor is used owing to its high sensitivity, and PVDF film is adopted to provide balanced stiffness and compliance for the sensing element. Although PVDF film can also provide a force sensing signal, the dynamic force sensor is not suitable for the measurement of microinjection force and sophisticated electrical circuit is needed to process the dynamic signal output of PVDF. While the implemented piezoresistive sensor is able to offer a stable measurement of the cell injection force.

3) FABRICATION OF THE CELL HOLDER

The proposed cell holder is fabricated using agarose rather than glass material. As a polymer material, agarose has been frequently employed in biological cell experiments. Such soft material can prevent the cell from damage and provide the cells with nutrients if necessary. The melting temperature of agarose is $90-95°C$, and it forms a semi-solid gel when the temperature drops to $34-38°C$. It is an ideal inert carrier. Considering the convenience and versatility, the cell holder is fabricated using agarose material. By adopting agarose material and a pre-designed mold, such cell holder is easy to fabricate. Agarose is hydrophilic and almost completely free of charged groups, and it rarely causes denaturation and adsorption to sensitive biological macromolecules.

4) HARDWARE COMPONENTS OF THE SYSTEM

The microinjection system has been developed by using the hardware components as described below. (a)

(a) A custom-built microinjection device with a piezoelectric stack actuator and a piezoresistive force sensor. More details can be referred to [13].
(b) An upright microscope (model: SZX16, from Olympus Inc.).
(c) A CCD Camera (model: MicroPublisher 5.0 RTV, from QImaging Corp.) with frame rate of 15 fps. It is used for real-time image acquisition and object location.
(d) An XYZ micromanipulator (model: MPC-385, from Sutter Instrument Company) with maximum travel range: 25 mm, maximum speed: 5 mm/s and step resolution: 0.25 μm. It is adopted for the position control of the microinjector.

(e) An XY positioning stage (model: MLS203-2P, from Thorlabs Inc.) with maximum travel range: 110 mm × 75 mm, maximum velocity: 250 mm/s and absolute on-axis accuracy < 3 μm. It is employed for position control of the supported petri dish.
(f) A picoliter microinjector (model: PLI-100A, from Warner Instruments Inc.) with injection pressure: 1.37–413 kPa and holding vacuum: 0–0.75 kPa. It is adopted for injecting drugs into cells.
(g) A real-time controller (model: cRIO 9075, from National Instrument Inc.) with 400 MHz CPU, 128 MB DRAM and 256 MB storage. It collects the sensor data, runs the position/force control algorithm, and drives the piezoelectric injector via a linear voltage amplifier (model: EPA-104-230, from Piezo Systems Inc.).
(h) A host computer (Intel Core-i7 CPU, maximum processing speed of 3.6 GHz with 16 GB RAM) running LabVIEW software.

The employed LabVIEW software provides the programming environment with several advantages as follows. a) The program is executed in parallel inherently by the dataflow programming. b) It offers rich function and toolbox. c) It supports a wide range of application programming interface (API) provided by various device manufacturers. Such advantages make it easier to develop the motion/force control system by combining multiple devices together.

B. PREPARATION OF CELLS AND INJECTED MATERIAL

Zebrafish embryos are adopted as biological cells in this work. The zebrafish embryos have been prepared according to the standard procedure.

Clustered regularly interspaced short palindromic repeats (CRISPR/Cas9) was originally discovered as part of the acquired immunity in bacteria and archaea. Recently, it has been developed as an effective approach for genome editing. The CRISPR/Cas9 system contains a single guiding RNA (sgRNA), which can recognize and bind the specific DNA sequence when assembled with the Cas9 endonuclease. The Cas9 enzyme will then cleave the bound DNA at the upstream of the protospacer adjacent motif sequence, leading to the mutation of the targeted DNA sequence [28].

In experimental study, the sgRNA and Cas9 mixture is injected into Zebrafish embryos to increase the rate of its gene mutation by cutting the gene sequence. With only the cutting and repairing operations, but no genes inserted, there will be a higher mutation rate of fertilized embryo. The new beneficial traits coming from the Zebrafish mutation is what we need in the concerned experiments. In this work, the drug dose of 2.2 nL is injected to every cell. The tip diameter of the adopted injector is 1 μm and the depth of injection is set as 700 μm.

III. DEVELOPMENT OF MACHINE VISION ALGORITHM AND CONTROL ALGORITHM

In order to realize automated cell injection precisely, the location of the cells must be obtained by sensors. For that, machine vision is adopted to provide the cell location [29]. As one of the popular pattern matching algorithms in machine vision, the template matching method is employed in this work to locate the cells and injector tip. The main idea of pattern matching is to compute the difference between each position of a target image and a given template image [30], [31]. The positions which give the lowest difference are considered as the matching result.

In view of the computational cost of such algorithm and the requirement on real-time locating, optimization schemes are needed. In this work, the Kalman filter (KF) and pyramid template matching (PTM) are combined to locate the objects. Specifically, the KF minimizes the searching region and the pyramid template matching algorithm further reduces the computation load. Once an uninjected cell is detected, it will be translated to a specified location where the injector tip can pierce with the help of cell-searching algorithm. The proportional-integral-derivative (PID) motion controller is applied in this phase for increasing the positioning accuracy and speed. The work flow of entire microinjection system is given in Fig. 3.

A. PYRAMID TEMPLATE MATCHING (PTM) ALGORITHM

Template matching method compares the difference between the object's image and template image. The measure of sum of squared differences (SSD) can be represented by [32]:

$$R_{SSD}(x, y) = \sum_{i,j}[I(x+i, y+j) - T(i,j)]^2 \tag{1}$$

where the pixel sizes of the object's image and template image are assumed to be $M_I \times N_I$ and $M_T \times N_T$ in gray scale, respectively. In addition, x and y are defined in the range of $[0, M_I - M_T]$ and $[0, N_I - N_T]$, respectively.

Using Eq. (1), a matrix is calculated, whose elements contain the matching differences at each position. If one or more matching points give rather low values, the corresponding positions are taken as the matched position.

In practice, there are some issues of computational cost and energy problem. The energy problem lies in that if the brightness of the object image changes, the matching method will give totally different results, which reduces the reliability of the algorithm. In order to overcome such problem, the normalized cross correlation (NCC) is employed as follows [33].

$$R_{NCC}(x, y) = \frac{\sum_{i,j}[I(x+i, y+j) - \bar{I}][T(i,j) - \bar{T}]}{\sqrt{\sum_{i,j}[I(x+i, y+j) - \bar{I}]^2 \sum_{i,j}[T(i,j) - \bar{T}]^2}} \tag{2}$$

The computational result of Eq. (2) can be regarded as a matrix, whose elements correspond to the matching results at the location. Because the areas that match the template will not be a single point and several points may be very close to each other, the duplicate locations are removed. Moreover, if multiple objects are searched in the image, there will be more than one group of points. In such cases, only the point with the highest value in each group is needed.

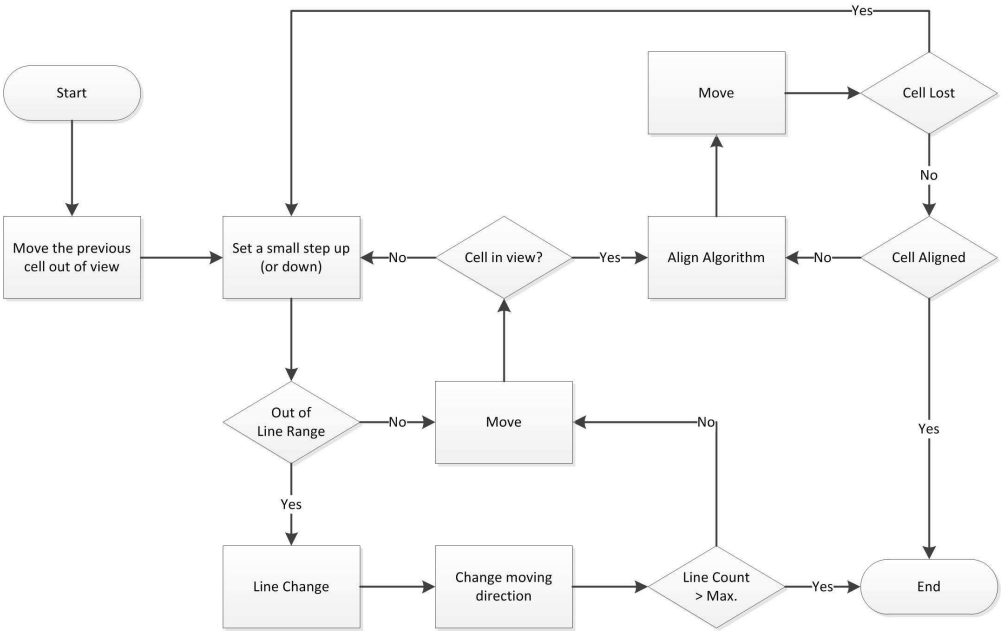

FIGURE 3. Flow chart of the overall microinjection system.

As mentioned above, Eq. (2) costs too much calculation time. Thus, the pyramid algorithm is employed, which is an optimization method for reducing the computational load of template matching. This algorithm transforms the matching image and the template image into several different sizes, and the smallest pair is computed first. In the smallest pair, the overall computational load is low, and a coarse position of the object is given. In the next larger pair, only the region that is close to the given position will be matched. Through such a coarse-to-fine process, the original image pair is matched. This algorithm reduces the computation cost of the matching by ignoring most of the area which does not match the template in the lowest resolution image [34].

Assume that a pyramid transfer equation is given by $f(x) = 1/2^x$, which represents the transfer size of every matching image pair. If the original matching pair is set as number 0, and the image size is described by S_{I0} and S_{T0}. Then, the image size of the matching pair with number n is calculated as:

$$S_{In} = f_{pr}(n) \times S_{I0} \tag{3}$$

$$S_{Tn} = f_{pr}(n) \times S_{T0} \tag{4}$$

Based on Eqs. (3) and (4), the pair of pyramid matching image can be generated.

Next, the PTM process for a single object detection is presented as follows.

(a) Generate all of the pyramid image pairs;
(b) Set $i = n$;
(c) Calculate the result matrix of the ith image;
(d) Select the mostly matched point;
(e) Restore the selected point's location P into a region I_{i-1}, and record it as ROI_{i-1};
(f) Repeat steps (III-A) to (III-A), until the object location of I_0 is obtained.

In step (III-A), the location of every point can be restored into a region, because when the ith image is generated, every pixel of the image comes from more than one pixel, and a region will be given when this transform is reversed.

B. KALMAN FILTER (KF) DESIGN

The KF is a widely employed adaptive filter which optimizes the parameters with iteration process [35]. With the help of the predicted estimate states and observation status, the system's real states can be estimated by the KF [36]. In this work, a 2-D KF is employed to predict the object's position for minimizing the detection time and reducing the detection noise.

As the object moving path in the tracking system is continuous in practice, its next position can only lie in a limited region. This region is mostly smaller than the field of view of the microscope. Thus, the KF, which filters the input data with an adaptive prediction equation, is a useful tool for the automated cell injection system in this work. The KF predicts the next possible location of the object and filters the object's location after running the PTM algorithm. The filter works for reducing the detection noise and avoiding the influence of mis-detection. At the end of the calculation process, the KF will upgrade itself to improve the performance.

The object movement function can be represented by:

$$\begin{bmatrix} X(k+1) \\ V(k+1) \end{bmatrix} = \begin{bmatrix} 1 \\ 0 \end{bmatrix} X(k) + \begin{bmatrix} \Delta T \\ 1 \end{bmatrix} \times V(k) + \begin{bmatrix} 0.5\Delta T^2 \\ \Delta T \end{bmatrix} a(k) \tag{5}$$

where $X(k)$, $V(k)$, and $a(k)$ are the object's position, velocity, and acceleration at the kth moment, respectively. ΔT is the sampling time interval.

Let $X_u = \begin{bmatrix} p_x & v_x & p_y & v_y \end{bmatrix}^T$ and X_p represent the current and predicted positions of the object. In addition, $F = \begin{bmatrix} 1 & \Delta T & 0 & 0 \\ 0 & 1 & 0 & 0 \\ 0 & 0 & 1 & \Delta T \\ 0 & 0 & 1 & 0 \end{bmatrix}$, $B = \begin{bmatrix} \Delta T^2/2 & 0 \\ \Delta T & 0 \\ 0 & \Delta T^2/2 \\ 0 & \Delta T \end{bmatrix}$, and $u = \begin{bmatrix} a_x & a_y \end{bmatrix}^T$. Then Eq. (5) can be rewritten as:

$$X_p = FX_u + Bu \tag{6}$$

which is called the state transfer equation [37].

Then, let Q represent the covariance of the process noise. The estimate covariance P_p in KF can be predicted as:

$$P_p = FP_uF^T + Q \tag{7}$$

Eqs. (5) and (7) are the prediction functions, which predict the object's position and system estimate covariance. Afterwards, the searching ROI for the PTM can be given, and the object is located by running the matching algorithm. If the object is located, then its position $z = \begin{bmatrix} p_x & p_y \end{bmatrix}^T$ will be sent to KF for filtering.

By combining the predicted system estimate and the detected location, the system estimate X_u and estimate covariance P_u can be updated by:

$$X_u = (I - KH)X_p + Kz \tag{8}$$

$$P_u = (I - KH)P_p \tag{9}$$

where I is the unit matrix and $H = \begin{bmatrix} 1 & 0 & 0 & 0 \\ 0 & 0 & 1 & 0 \end{bmatrix}$ is called the observation model. It governs the relationship of the transform between X and z by:

$$z = HX \tag{10}$$

where K is called Kalman gain, which can be obtained by

$$K = P_pH^T(HP_pH^T + R)^{-1} \tag{11}$$

where R is the covariance of the observation noise. Its value can be obtained by conducting preliminary experiment. Then, one iteration process of the KF is finished.

The five equations of KF can be divided into two parts—the prediction part (see Eqs. (5) and (7)) and filtering part (see Eqs. (8), (9), and (11)). At each iteration of KF, the Kalman gain is computed by the predicted covariance estimate and observation noise covariance (see Eq. (11)). Then, the detected location from PTM is combined with the predicted estimate state using Eq. (8). The computational result, i.e., estimated state, contains the finally filtered object location. The covariance estimate is also upgraded based on its prediction and Kalman gain by Eq. (9). Hence, the filtering part is completed. Afterwards, the next estimate state is predicted based on the previous state by Eq. (7). This state contains the predicted next location of the object, and will be sent to PTM for generating the matching ROI. The estimate covariance is predicted with Eq. (7). Thus, the current KF iteration is finished.

C. PROPOSED IMAGE PROCESSING ALGORITHM DESIGN

In this work, the PTM is combined with KF filter to speed up the image processing speed. As mentioned earlier, the KF is divided into two parts. The prediction part gives the object's position based on the previous movement path. This predicted position is set as a center of the object detection ROI. So, the PTM can start to search the object in this ROI, and the corrected position of the object will be sent to the KF for noise minimization, once the object is detected. Afterwards, the object's position is used by the controller for motion control. Meanwhile, the parameters of KF will be upgraded for a better performance of prediction and filtering.

IV. EXPERIMENTAL RESULTS

In this section, experimental study is carried out to inject a batch of cells using the developed automated cell microinjection system.

A. CALIBRATION RESULTS

Assume that the distortion coefficient of the employed camera is 0, the transformation matrix T between the camera coordinate and the world coordinate can be simply represented by:

$$X_w = TX_c \tag{12}$$

where $X_w = [x_w, y_w, 1]^T$ is the location of the object in the world coordinate, and $X_c = [x_c, y_c, 1]^T$ is the location in the camera coordinate. To obtain the transformation matrix T, a cell is placed in the field of view. Then, the cell is positioned to track a circular trajectory by driving the XY positioning stage. The circle path is selected to cover the camera's field of view as large as possible to minimize the calibration error arising from the image distortion.

As shown in Fig. 2(c)–(d), the fitting result matches the observation result well. The transformation matrix T is given by:

$$T = \begin{bmatrix} 0.01034 & 0 & -2.224 \times 10^{-13} \\ 0 & -0.01032 & 4.249 \times 10^{-13} \\ 0 & 0 & 1 \end{bmatrix}$$

While the object is fixed at a given location, the locations obtained by the object detection algorithm are recorded and counted as shown in Fig. 2(e)–(f). It is observed that the object detection noise follows a normal distribution in both x- and y-axes. The standard deviations are $\sigma = 1.918 \times 10^{-4}$ μm and $\sigma = 2.136 \times 10^{-4}$ μm for x- and y-axes, respectively. Thus, the 2σ resolutions [38] of detection are calculated as 0.3836 μm and 0.4272 μm for the x- and y-axes, respectively.

In this system, the employed piezoresistive force sensor is based on semiconductor strain gauge, which provides analog voltage signal output by a half-Wheatstone bridge circuit. It is assumed that the relationship between the piercing force and voltage output is linear. Thus, the force gain can be calibrated

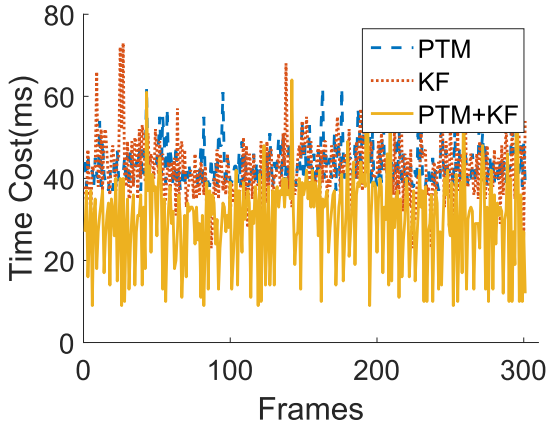

FIGURE 4. Calculation time of different algorithms for object locating.

by using a commercial force sensor with force signal output. The relationship is given as

$$F = \begin{bmatrix} a_1 & a_0 \end{bmatrix} \begin{bmatrix} v \\ 1 \end{bmatrix} \tag{13}$$

where a_1 and a_0 are the coefficients of the linear function, and v is the output voltage of the strain-gauge force sensor.

In the calibration experiment, the force signal (from commercial force sensor) and strain-gauge output signal are acquired as shown in the Fig. 2(b) (blue dots). The red line represents the fitted linear curve. It is seen that the fitted curve matches the experimental result well. The linear function's coefficients are determined as $a_1 = -20019.6$ and $a_0 = -40.2$. In addition, the 2σ resolution of the calibrated force sensor is about 0.2 mN.

B. CELL LOCATING RESULTS WITH MACHINE VISION ALGORITHMS

To demonstrate the performance of proposed combination approach (PTM+KF) for locating the cells, experimental study is conducted to compare the performances of PTM, KF, and PTM+KF methods. In these experiments, the cells in petri dish are supported and translated by the XY positioning stage to move along a given trajectory. For illustration, a circular trajectory with the diameter of 100 μm is planned to be completed in 20 s. A frame rate of 15 fps is implemented. The time required by each algorithm in every step is recorded and depicted as shown in Fig. 4.

As compared with the original PM approach which requires an average calculation time of 814.79 ms, both PTM and KF algorithms significantly reduce the average computation time to around 43 ms. Relatively, the KF method is more stable than PTM, as KF leads to a smaller standard deviation (5.36 ms) than the PTM result (7.70 ms). Moreover, the proposed PTM+KF approach further reduces the average computation time to 29.85 ms with the standard deviation of 11.00 ms. Hence, in comparison with individual PTM and KF algorithms, the combined PTM+KF algorithm reduces the average calculation time by 30%.

C. CELL DETECTION AND SEARCHING RESULTS WITH MACHINE VISION BASED FEEDBACK CONTROL

The cell-searching process is realized in two steps, i.e., the pre-searching and object alignment. The pre-searching procedure is used to translate the petri dish by following a generated path (see Fig. 5(a)), and to match the overall searching region of interest (ROI) for determining whether a cell comes into the field of view by the detection algorithm. This procedure is run until a new cell is detected or all of the searching paths have been finished. The petri dish translates with small steps while the object detection algorithm finds the cell from the captured image. If a cell is detected, the petri dish will stop translating and the alignment algorithm begins.

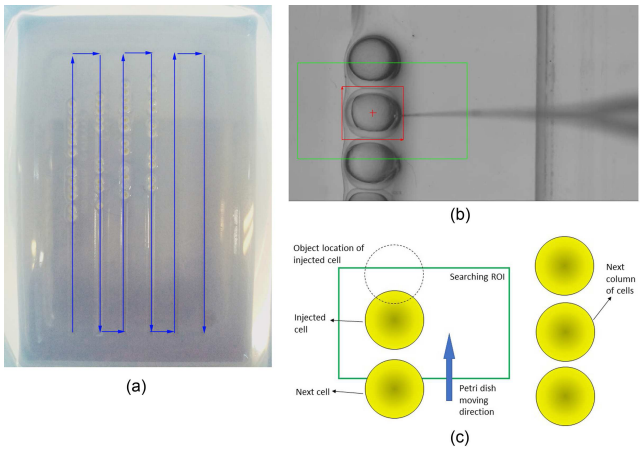

FIGURE 5. (a) The cell searching path in the petri dish; (b) ROI in the searching process; (c) schematic diagram.

The alignment algorithm is implemented to align the cell's position to the place that faces the injector tip. In order to align the object cell reliably and efficiently, a 2-D PID closed-loop controller (for x and y positions) is adopted along with the object detection algorithm. The detection algorithm calculates the distance between the cell and the object location as the input of PID controller, and the PID controller drives the XY positioning stage (supporting the petri dish) in a closed-loop way. The control action is expressed as follows.

$$M = EP = \begin{bmatrix} e_x & \int_0^t e_x d\tau & \dot{e_x} & e_y & \int_0^t e_y d\tau & \dot{e_y} \end{bmatrix} \begin{bmatrix} p_x & 0 \\ i_x & 0 \\ d_x & 0 \\ 0 & p_y \\ 0 & i_y \\ 0 & d_y \end{bmatrix} \tag{14}$$

where the control gains p_x, i_x, d_x, p_y, i_y, and d_y are tuned by trial-and-error in experiments.

These steps are run several times to ensure that the alignment error is reduced. Aiming at a better adaptability,

the special situations (such as object lost, cell line shift, and auto-stop) are treated as follows.

1) OBJECT LOST

In practice, there may be some scenarios where the controller works wrongly or the object (cell) is mis-detected, such that the object is lost even if the pre-searching process locates a new object. The object lost function will lead the system to search a new cell if the object detection algorithm cannot find a cell from a specified number of continuous frames of the image in the cell alignment process.

2) SHIFT OF CELL LINE

When all of the cells in the current line have been injected, the line shift function leads the next line of cells in the petri dish to the field of view. Once the petri dish (driven by an XY positioning stage) moves out of the up and bottom limits of each line, it can be determined that the current line of cells are injected completely, and the next line of cells need to be moved into the field of view. Meanwhile, the searching direction will be turned into the opposite direction.

3) AUTO-STOP

Every time when the function of cell line shift is triggered, the auto-stop function works before the move command is sent to the XY positioning stage. In this function, if the count of cell lines is larger than the assigned maximum value, the petri dish will not move to a new line. Instead, the system will be turned to stop status.

As shown in Fig. 5(b), the maximum searching ROI for object detection in the system is only a part of the microscope's field of view. Limiting the boundary of the searching ROI is a simple and effective method, because the detection algorithm will provide all of the detected objects which match the template.

Referring to Fig. 5(c), these limitations can be overcome by the following conditions. (a) At least one complete cell can be located for the object detection algorithm; (b) There is enough space for cell alignment; (c) There will be no cases where two cells come into the searching ROI; (d) The cell in other lines will not come into the ROI.

Let H_{ROI} and W_{ROI} represent the height and width of the boundary for the maximum searching ROI. In addition, R_c is the average radius of the target cells, and D_{col} is the distance between two cell lines. The limits of the maximum searching ROI can be defined bellow:

$$2R_c < H_{ROI} < 4R_c \tag{15}$$

$$R_c < W_{ROI} < D_{col} \tag{16}$$

Once a cell is injected, it is moved out of the field of view quickly, so as to search the next cell. This also avoids the case that the injected cell is misunderstood as a new target cell by the controller after several moving steps. As the current cell's position and ROI boundary are known, a new position that is a fraction of the object (just out of the boundary as denoted by dotted circle in Fig. 5(c)) can be given, and its moving distance is easy to obtain. The controller will send a command to XY stage based on the moving step, so that the currently injected cell will just move to the given position. However, if the searching direction is from top to bottom, the boundary will be selected as the bottom one of the searching ROI. Then, the next cell searching process starts. In majority of situations where the cells are placed quite close to each other, the next cell will be located immediately when the previous one is moved out of the field of view. This new cell will be aligned and injected. If no cell is found, the XY stage will be controlled to move quickly until a cell is detected.

D. FORCE-SENSING CELL INJECTION RESULTS WITH MOTION CONTROL

After the cell is translated to the target position, the cell injection operation starts. In this phase, the injector is guided to pierce the cell membrane with force sensing and to inject drug into the cell. Based on the differential force signal, the controller can judge whether the cell membrane is pierced or the injection process fails. If the cell is pierced successfully, the drug injector driver will be triggered. Otherwise, the controller will continue to impose piercing force or stop the piercing and searching for a new cell for injecting. This strategy is used to make sure that the cell is always penetrated.

The overall motion control process of the system is divided into the following steps. (a) Initializing the system parameters; (b) Searching a new cell to inject; (c) Aligning the cell location; (d) Piercing the cell membrane; (e) Injecting drug into cell; (f) Retracting the injector for protecting the cell and injector; (g) Repeating steps (b)–(f) until all of cells are injected.

The cell injection process consists of three phases, i.e., cell piercing, drug injecting, and injector pulling out. In the cell piercing phase, force sensing is implemented for cell protection and status judgment. During the cell piercing process, the injector is driven to translate at a constant speed until the stop signal is given. The injection force will continually increase if the injector tip touches the cell membrane. If the cell membrane is pierced, there will be an obvious step change signal in the force signal, and a high peak of differential force signal will appear at this moment. However, if the cell membrane is not pierced, the differential force signal will keep in a small range. So, the differential force signal is calculated and fed back to determine whether the cell membrane is pierced or not. The threshold value of differential force is set based on experimental study. Moreover, both injection force limit and injection distance limit are assigned. Such limits will protect the injected cells from being scratched.

The snapshots of the cell piercing process are shown in Fig. 6. As mentioned earlier, the system searches a new un-injected cell first. If a cell comes into the field of view (see Fig. 6(a)), the cell will be positioned close to the injector tip (see Fig. 6(b)). Then, the controller drives the injector pipette to pierce the cell membrane (see Fig. 6(c)) until the

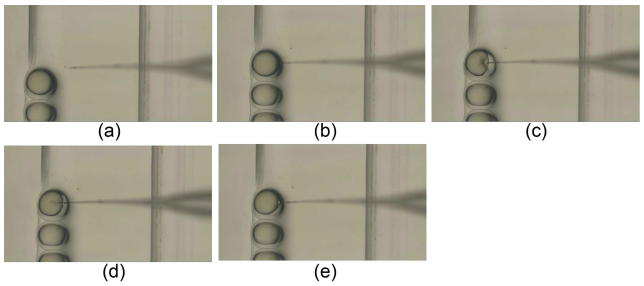

FIGURE 6. Snapshots of the cell injection process. (a) A cell is translated into the field of view. (b) The cell is aligned close to the injector tip. (c) The injector is driven to pierce the cell membrane. (d) Cell membrane is pierced by the injector. (e) The injector is retracted.

membrane is pierced (see Fig. 6(d)). In the piercing process, as the cell shape changes, the injecting force starts to increase (see Fig. 7). At the moment when the cell membrane is pierced successfully, the injecting force will decrease to zero drastically, which is indicated by the force signal of injection. Once the cell is pierced, the drug material will be injected into the cell. At the end of the process, the injector is retracted (see Fig. 6(e)), and the searching process of the next cell starts.

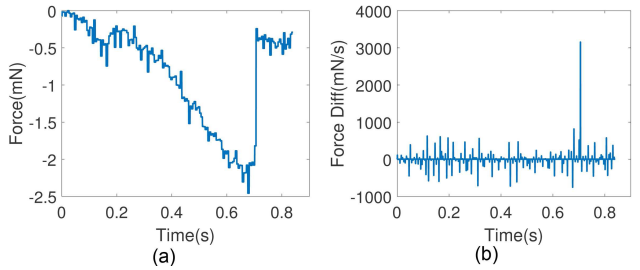

FIGURE 7. (a) Force sensor output signal in the piercing process. (b) Differential force signal in the piercing process.

In the cell piercing process, when the injector is driven to pierce into the cell with a constant speed, the imposed force signal is measured by the force sensor. Fig. 7 gives typical force sensing result and the corresponding differential force signal in the cell piercing process. It is seen that there is a step change in the force signal around 0.704 s, as shown in Fig. 7(a). At this moment, the cell membrane is pierced and the piercing force reduces to zero instantly. The force signal serves as a good feature to judge whether the cell membrane is pierced or not. In addition, the differential force signal is the indicator of the piercing status, as illustrated in Fig. 7(b). Thus, if the differential force is larger than the given threshold, the piercing process is considered to be completed and the injection process of the next cell will be conducted. In this work, the judgment threshold is assigned as 2000 mN/s.

E. DISCUSSIONS

The experiment has been repeated by 5 times. In each times of experiment, a batch of 69 cells are injected by the automated microinjection system. For comparison, the same operation is also conducted by a skilled human operator who has more than three years' manual injection experience. The total sample size is 690 and the statistical results are shown in Fig. 8. The average results of the injection speed and cell viability are tabulated in Table 1.

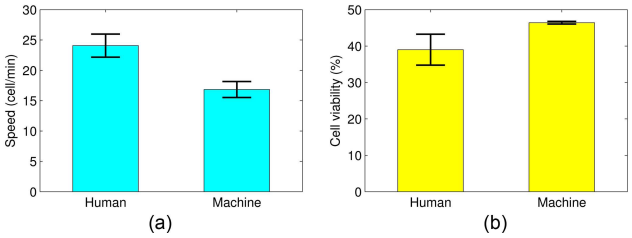

FIGURE 8. Cell microinjection results of the automated machine and human operator. (a) Injection speed; (b) cell viability.

TABLE 1. Cell injection results.

Performance	Cell microinjection system	Human operator
Injection speed	3.55 s/cell	2.50 s/cell
Cell viability	46.0%	39.0%

Results indicate that the developed microinjection system provides the average injection speed of 3.55 s per cell, which is 42% slower than the skilled manual speed of 2.50 s per cell. On the other hand, the results reveal that the automated system achieves the average cell viability of 46.0%, which is 18% higher than the manual operation result of 39.0%. The cell viability is calculated as the ratio between the number of survived cells after injection and the total number of injected cells. Moreover, concerning the cell viability, the standard deviation of the microinjection system's result is 0.37, which has been reduced by 91% in comparison with the manual operation result of 4.24.

Considering that the injection speed of the automated system can be greatly enhanced by employing multiple machines working in parallel, the developed microinjection system is superior to manual manipulation in terms of consistency and viability of the injected cells, which are the key indicators of the cell injection quality. Therefore, the experimental results confirm the effectiveness of the developed force-sensing microinjection system for multi-cell injection task.

Moreover, the proposed cell holder is also beneficial to cell placement. If the designed inclined grooves are close to each other, and then the cells can slide directly into the grooves and achieve self-immobilization. Thus, it is no longer necessary to manually arrange cells one by one. This greatly improves the overall operation efficiency. In the future work, the overall operation time will be considered to reveal the advantage of the presented cell holding device. Additionally, in the future work, the resolution of the force sensor will be enhanced by adopting more sophisticated signal conditioning circuit and the injection speed of the system will be improved by

employing more advanced image acquisition and processing hardware.

V. CONCLUSION

This paper presents an automated multi-cell microinjection system with force sensing capability for genome editing of zebrafish. A new type of cell holder is introduced to immobilize the cells, which speeds up the process of cell injection. The pyramid template matching approach combined with Kalman filter is employed to improve the matching speed and enables a higher performance of position control without influencing the detection resolution. Experimental results show that the presented combination method reduces the average computation time by 30% in comparison with PTM or KF methods. The injecting force is measured to judge whether the cell membrane is pierced or not. The cells are also protected based on the force sensing. Aiming at increasing the applicability of the developed system, several special scenarios have been considered. Experimental results reveal the effectiveness of the force-sensing microinjection system over skilled human operator in multi-cell injection task. In the future work, the system will be further improved and adopted to conduct more types of cell manipulation tasks.

REFERENCES

[1] W. Wang, X. Liu, D. Gelinas, B. Ciruna, and Y. Sun, "A fully automated robotic system for microinjection of zebrafish embryos," *PLoS ONE*, vol. 2, no. 9, p. e862, 2007.
[2] S. Permana, E. Grant, G. M. Walker, and J. A. Yoder, "A review of automated microinjection systems for single cells in the embryogenesis stage," *IEEE/ASME Trans. Mechatronics*, vol. 21, no. 5, pp. 2391–2404, Oct. 2016.
[3] R. J. Wall, "Pronuclear microinjection," *Cloning Stem Cells*, vol. 3, no. 4, pp. 209–220, 2001.
[4] H. Ladjal, J.-L. Hanus, and A. Ferreira, "Micro-to-nano biomechanical modeling for assisted biological cell injection," *IEEE Trans. Biomed. Eng.*, vol. 60, no. 9, pp. 2461–2471, Sep. 2013.
[5] C. Leung, Z. Lu, N. Esfandiari, R. F. Casper, and Y. Sun, "Automated sperm immobilization for intracytoplasmic sperm injection," *IEEE Trans. Biomed. Eng.*, vol. 58, no. 4, pp. 935–942, Apr. 2011.
[6] J. Liu *et al.*, "Robotic adherent cell injection for characterizing cell–cell communication," *IEEE Trans. Biomed. Eng.*, vol. 62, no. 1, pp. 119–125, Jan. 2015.
[7] Z. Wang, C. Feng, R. Muruganandam, W. T. Ang, S. Y. M. Tan, and W. T. Latt, "Three-dimensional cell rotation with fluidic flow-controlled cell manipulating device," *IEEE/ASME Trans. Mechatronics*, vol. 21, no. 4, pp. 1995–2003, Aug. 2016.
[8] G. Hwang, C. Preeda, and H. Hashimoto, "Developing intelligent robotic biomanipulation system using haptic interface," in *Proc. 2nd IEEE Int. Conf. Nano/Micro Eng. Mol. Syst. (NEMS)*, Bangkok, Thailand, Jan. 2007, pp. 396–401.
[9] L. Ren, L. Wang, J. K. Mills, and D. Sun, "Vision-based 2-D automatic micrograsping using coarse-to-fine grasping strategy," *IEEE Trans. Ind. Electron.*, vol. 55, no. 9, pp. 3324–3331, Sep. 2008.
[10] Q. Xu, *Micromachines for Biological Micromanipulation*. Cham, Switzerland: Springer, 2018.
[11] Y. Zhang, K. K. Tan, and S. Huang, "Vision-servo system for automated cell injection," *IEEE Trans. Ind. Electron.*, vol. 56, no. 1, pp. 231–238, Jan. 2009.
[12] K. Sakaki, N. Dechev, R. Burke, and E. Park, "Development of an autonomous biological cell manipulator with single-cell electroporation and visual servoing capabilities," *IEEE Trans. Biomed. Eng.*, vol. 56, no. 8, pp. 2064–2074, Aug. 2009.
[13] G. Wang and Q. Xu, "Design and development of a piezo-driven microinjection system with force feedback," *Adv. Robot.*, vol. 31, nos. 23–24, pp. 1349–1359, 2017.
[14] W. Zhang, A. Sobolevski, B. Li, Y. Rao, and X. Liu, "An automated force-controlled robotic micromanipulation system for mechanotransduction studies of Drosophila larvae," *IEEE Trans. Autom. Sci. Eng.*, vol. 13, no. 2, pp. 789–797, Apr. 2016.
[15] M. A. Greminger and B. J. Nelson, "Vision-based force measurement," *IEEE Trans. Pattern Anal. Mach. Intell.*, vol. 26, no. 3, pp. 290–298, Mar. 2004.
[16] X. Liu, K. Kim, Y. Zhang, and Y. Sun, "Nanonewton force sensing and control in microrobotic cell manipulation," *Int. J. Robot. Res.*, vol. 28, no. 8, pp. 1065–1076, 2009.
[17] J. Kim, F. Janabi-Sharifi, and J. Kim, "A haptic interaction method using visual information and physically based modeling," *IEEE/ASME Trans. Mechatronics*, vol. 15, no. 4, pp. 636–645, Aug. 2010.
[18] Y. Tan, D. Sun, W. Huang, and S. H. Cheng, "Mechanical modeling of biological cells in microinjection," *IEEE Trans. Nanobiosci.*, vol. 7, no. 4, pp. 257–266, Dec. 2008.
[19] Y. Wei and Q. Xu, "An overview of micro-force sensing techniques," *Sens. Actuators A, Phys.*, vol. 234, pp. 359–374, Oct. 2015.
[20] Z. Lu, P. C. Y. Chen, J. Nam, R. Ge, and W. Lin, "A micromanipulation system with dynamic force-feedback for automatic batch microinjection," *J. Micromech. Microeng.*, vol. 17, no. 2, pp. 314–321, 2007.
[21] Y. Wei and Q. Xu, "Design of a PVDF-MFC force sensor for robot-assisted single cell microinjection," *IEEE Sensors J.*, vol. 17, no. 13, pp. 3975–3982, Jul. 2017.
[22] Y. Xie, D. Sun, C. Liu, H. Y. Tse, and S. H. Cheng, "A force control approach to a robot-assisted cell microinjection system," *Int. J. Robot. Res.*, vol. 29, no. 9, pp. 1222–1232, 2010.
[23] Y. Xie, D. Sun, H. Y. G. Tse, C. Liu, and S. H. Cheng, "Force sensing and manipulation strategy in robot-assisted microinjection on zebrafish embryos," *IEEE/ASME Trans. Mechatronics,* vol. 16, no. 6, pp. 1002–1010, Dec. 2011.
[24] Y. Sun and B. J. Nelson, "Biological cell injection using an autonomous microrobotic system," *Int. J. Robot. Res.*, vol. 21, nos. 10–11, pp. 861–868, 2002.
[25] Q. Du, Q. Zhang, L. Tian, and Z. Wu, "Object detection and tracking for a vision guided automated suspended cell injection process," in *Proc. Int. Conf. Mechatronics Autom. (ICMA)*, Xi'an, China, Aug. 2010, pp. 1760–1764.
[26] H. B. Huang, D. Sun, J. K. Mills, and S. H. Cheng, "Robotic cell injection system with position and force control: Toward automatic batch biomanipulation," *IEEE Trans. Robot.*, vol. 25, no. 3, pp. 727–737, Jun. 2009.
[27] Z. Lu, X. Zhang, C. Leung, N. Esfandiari, R. F. Casper, and Y. Sun, "Robotic ICSI (intracytoplasmic sperm injection)," *IEEE Trans. Biomed. Eng.*, vol. 58, no. 7, pp. 2102–2108, Jul. 2011.
[28] R. Barrangou, "Diversity of CRISPR-Cas immune systems and molecular machines," *Genome Biol.*, vol. 16, no. 1, p. 247, 2015.
[29] X. Yin, G. Jiang, and S. Song, "Research on an automatic tracking strategy based on CCD image sensor in micromanipulation," *IEEE Access*, vol. 6, pp. 76374–76380, 2018.
[30] M. Graves and B. Batchelor, *Machine Vision for the Inspection of Natural Products*. London, U.K.: Springer, 2003.
[31] Z. Lu, P. C. Y. Chen, and W. Lin, "Force sensing and control in micromanipulation," *IEEE Trans. Syst., Man, Cybern. C, Appl. Rev.*, vol. 36, no. 6, pp. 713–724, Nov. 2006.
[32] J. P. Lewis, "Fast template matching," *Vis. Interface*, vol. 95, pp. 120–123, May 1995.
[33] K. Briechle and U. D. Hanebeck, "Template matching using fast normalized cross correlation," *Proc. SPIE*, vol. 4387, pp. 95–102, Mar. 2001.
[34] E. H. Adelson, C. H. Anderson, J. R. Bergen, P. J. Burt, and J. M. Ogden, "Pyramid methods in image processing," *RCA Eng.*, vol. 29, no. 6, pp. 33–41, 1984.
[35] D. M. Wolpert and Z. Ghahramani, "Computational principles of movement neuroscience," *Nature Neurosci.*, vol. 3, pp. 1212–1217, Nov. 2000.
[36] G. S. Gupta, C. H. Messom, and S. Demidenko, "Real-time identification and predictive control of fast mobile robots using global vision sensing," *IEEE Trans. Instrum. Meas.*, vol. 54, no. 1, pp. 200–214, Feb. 2005.
[37] M. R. Rajamani, "Data-based techniques to improve state estimation in model predictive control," Ph.D. dissertation, Chem. Eng., Univ. Wisconsin-Madison, Madison, WI, USA, 2007.
[38] Q. Xu, "Design and development of a novel compliant gripper with integrated position and grasping/interaction force sensing," *IEEE Trans. Autom. Sci. Eng.*, vol. 14, no. 3, pp. 1415–1428, Jul. 2017.

ZHIJIE NAN received the B.S. degree in process equipment and control engineering from the North University of China, Taiyuan, Shanxi, China, in 2016. He is currently pursuing the M.S. degree in electromechanical engineering with the University of Macau, Macau, China. His current research interests include micro/nano-robotics, biological cell microinjection, and machine vision.

QINGSONG XU (M'09–SM'15) received the B.S. degree (Hons.) in mechatronics engineering from the Beijing Institute of Technology, Beijing, China, in 2002, and the M.S. and Ph.D. degrees in electromechanical engineering from the University of Macau, Macau, China, in 2004 and 2008, respectively. He was a Visiting Scholar with the University of California at Los Angeles, Los Angeles, CA, USA, RMIT University, Melbourne, VIC, Australia, the National University of Singapore, Singapore, and the Swiss Federal Institute of Technology, Zurich, Switzerland. He is currently an Associate Professor of electromechanical engineering with the University of Macau, where he directs the Smart and Micro/Nano Systems Laboratory. His current research interests include micro/nano-systems, micro/nano-mechatronics, robotics and automation, smart materials and structures, and computational intelligence. He is a member of the American Society of Mechanical Engineers (ASME). He is a Technical Editor of the IEEE/ASME TRANSACTIONS ON MECHATRONICS and an Associate Editor of the IEEE TRANSACTIONS ON AUTOMATION SCIENCE AND ENGINEERING, the IEEE ROBOTICS AND AUTOMATION LETTERS, and the *International Journal of Advanced Robotic Systems*.

YIBO ZHANG received the Ph.D. degree in health sciences from the University of Macau, Macau, China, in 2019. His research interests include CRISPR/Cas, gene knockout, homologous recombination, site-directed mutagenesis, and zebrafish.

WEI GE received the B.S. degree in experiment zoology from Nanjing University, Nanjing, China, in 1982, the M.S. degree in genetics from the Chinese Academy of Science (CAS), in 1985, and the Ph.D. degree in physiology from the University of Alberta, Canada, in 1993. He joined The Chinese University of Hong Kong, Hong Kong, in 1995, after spending two years doing postdoctoral research at the National Institute for Basic Biology (NIBB), Japan. He is currently a Chair Professor with the Faculty of Health Sciences, University of Macau, Macau, China, where he is the Head of the Centre of Reproduction, Development and Aging. Before joining the University of Macau, in 2013, he was a Full Professor with the School of Life Sciences, The Chinese University of Hong Kong. His research focuses on the functional analysis of the brain-pituitary-ovary axis using zebrafish as the model. His current research interests include endocrine regulation of reproduction by the reproductive and growth axes; intra-follicular paracrine/autocrine communication networks in the ovary; impacts of environmental endocrine-disrupting chemicals (EDCs) on reproduction and public health; and zebrafish as a model for aging, human diseases, and drug discovery.